

# We are IntechOpen, the world's leading publisher of Open Access books Built by scientists, for scientists

6,900

Open access books available

185,000

International authors and editors

200M

Downloads

Our authors are among the

154

Countries delivered to

TOP 1%

most cited scientists

12.2%

Contributors from top 500 universities



WEB OF SCIENCE™

Selection of our books indexed in the Book Citation Index  
in Web of Science™ Core Collection (BKCI)

Interested in publishing with us?  
Contact [book.department@intechopen.com](mailto:book.department@intechopen.com)

Numbers displayed above are based on latest data collected.  
For more information visit [www.intechopen.com](http://www.intechopen.com)



# Electrical Field Distribution along HVDC GIL Spacer in SF<sub>6</sub>/N<sub>2</sub> Gaseous Mixture

*Boxue Du, Jin Li and Hucheng Liang*

## Abstract

Many researchers have proposed a variety of mathematical models to simulate the surface charge accumulation process of DC-GIS/GIL spacers. However, few of them took the gas collision ionization and charge trapping-detrapping process into consideration. This chapter combined the plasma hydrodynamics and charge transport equations and built a modified model. Some conclusions are shown as follows: for the basin-type spacer, the surface charge has the same polarity as the applied voltage on the lower surface but the opposite polarity on the upper surface. For the disc-type spacer, the surface charge has the same polarity as the applied voltage near the shell but the opposite polarity near the conductor under negative voltage. But under positive voltage, negative charge exists almost on the whole surface. The most serious distortion of the electric field occurs at the triple junction of epoxy spacer. Under load condition, there is an obvious temperature rise on the conductor due to joule heating, which has a great influence on the electric field distribution. The application of shielding electrodes has the function of field grading at the triple junction, which can be referred in the DC GIS/GIL design.

**Keywords:** DC-GIS/GIL, epoxy spacer, temperature, surface charge accumulation, electric field distribution, shielding electrode

## 1. Introduction

Over the last few decades, the high voltage direct-current (HVDC) transmission technology have been developed to carry out long distance and high capacity power transmission [1, 2]. Thanks to their high reliability and low footprint, Gas Insulated Switchgears and Gas Insulated Lines (GIS/GIL) have been widely used in AC power system but scarcely in DC system [3, 4]. One important reason is that surface charge is easy to accumulate on the spacer surface under DC voltage, which leads to a substantial electric field distortion and even flashover faults [5]. Therefore, the surface charge accumulation and electric field distribution along the GIS/GIL spacers need to be understood.

In order to improve the reliability of GIS/GIL, researches aiming on the surface charge measurement and simulation have been conducted worldwide [6–8]. Some researchers built a scaled-down GIS/GIL and measured the surface charge distribution on the spacers [9–12]. Their measurements were conducted offline because the applied voltage on the conductor can easily cause damage to the electrostatic probe. The poor accuracy of offline measurement makes their measurements differ from

each other. Besides, the accumulated surface charge at the triple junction can hardly be detected by the probe, which actually has a very significant effect on the electric field distribution.

Simulation is another way to study the surface charge distribution on spacers. Many researchers have proposed a variety of mathematical models to simulate the surface charge accumulation process [13–17]. However, few of them took the gas collision ionization and charge trapping-detrapping process into consideration. This paper detailed the corona discharge and charge trapping-detrapping process by combining the plasma hydrodynamics and charge trapping-detrapping equations together. Under load conditions, GIS/GIL has an obvious temperature rise on the conductor. Considering there are many temperature-dependent factors in the surface charge accumulation process, the heat transfer equations are also coupled in this model to obtain the temperature distribution. Besides, the effects of shielding electrodes on the distorted electric field distribution are also studied.

## 2. Mathematical model

### 2.1 Geometric model

**Figure 1** shows the geometric models of GIS with different spacer structures. There are two commonly used types of spacers as shown in **Figure 1a** which is shaped like a basin and **Figure 1b** which is shaped like a disc. In the simulation, the external diameter of the central conductor is set to 60 mm and the internal diameter of the shell is set to 330 mm. DC  $\pm 320$  kV is applied on the central conductor and the shell is grounded.

### 2.2 Corona discharge in SF<sub>6</sub>/N<sub>2</sub> mixture

In this paper, the SF<sub>6</sub>/N<sub>2</sub> mixture is set as the insulating gas in GIS. The percentage of SF<sub>6</sub> is set to 50% and the pressure is set to 0.5 MPa.

The drift-diffusion process of the electron density  $n_e$  and electron energy density  $n_\epsilon$  can be described as [18],

$$\frac{\partial}{\partial t}(n_e) + \nabla \cdot \left[ -n_e \left( \mu_e \cdot \vec{E} \right) - D_e \cdot \nabla n_e \right] = R_e \quad (1)$$

$$\frac{\partial}{\partial t}(n_\epsilon) + \nabla \cdot \left[ -n_\epsilon \left( \mu_\epsilon \cdot \vec{E} \right) - D_\epsilon \cdot \nabla n_\epsilon \right] + E \cdot \Gamma_e = R_\epsilon \quad (2)$$

where the electron mobility  $\mu_e$ , electron diffusivity  $D_e$ , energy mobility  $\mu_\epsilon$  and energy diffusivity  $D_\epsilon$  are computed by solving the Two-term Boltzmann

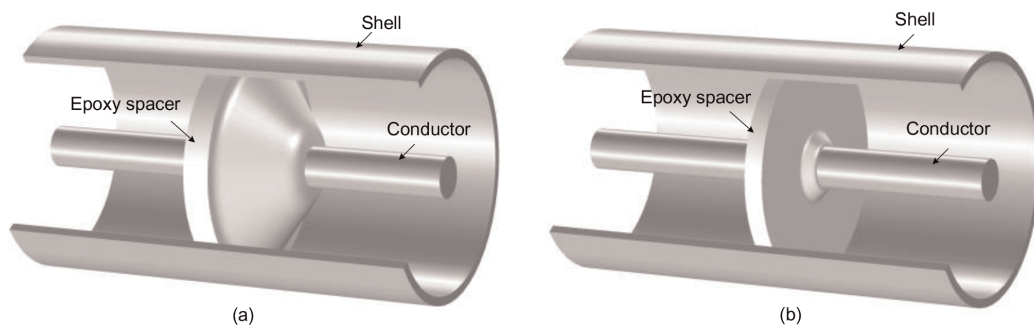


**Figure 1.**

The geometric models of GIS with different spacer structures: (a) basin-type and (b) disc-type.

equation [19]. The electron source  $R_e$  and energy source  $R_\epsilon$  can be obtained from Eqs. (3) and (4). This paper takes into consideration  $M$  electron-participating reactions ( $N$  two-body reactions and  $M-N$  three body reactions) and  $P$  energy-losing reactions,

$$R_e = \sum_{j=1}^N x_j k_j N_n n_e \Delta n_{ej} + \sum_{j=N+1}^M x_{j1} x_{j2} k_j N_n^2 n_e \Delta n_{ej} \quad (3)$$

$$R_\epsilon = \sum_{j=1}^P x_j k_j N_n n_e \Delta \epsilon_j \quad (4)$$

$$N_n = p/k_B T \quad (5)$$

where  $x_j$ ,  $x_{j1}$  and  $x_{j2}$  are the mole fractions of the target species for reaction  $j$ ;  $N_n$  is the total neutral density (1/m<sup>3</sup>);  $p$  is the gas pressure (Pa);  $T$  is the temperature (K);  $\Delta n_{ej}$  is the electron increment of reaction  $j$ ;  $\Delta \epsilon_j$  is the energy loss of reaction  $j$  (V) and  $k_j$  is the rate coefficient for reaction  $j$  (m<sup>3</sup>/s), which is also obtained from the two-term Boltzmann equation [19].

For heavy species, the space-time dependent mass fraction of species  $k$  is controlled by the following equations,

$$\rho \frac{\partial}{\partial t} (w_k) - \nabla \cdot \vec{j}_k = R_k \quad (6)$$

$$\vec{j}_k = \rho w_k \vec{V}_k \quad (7)$$

$$\vec{V}_k = D_k \left( \frac{\nabla w_k}{w_k} + \frac{\nabla M_n}{M_n} \right) - z_k \mu_k \vec{E} \quad (8)$$

where  $\rho$  is the gas density (kg/m<sup>3</sup>);  $w_k$  is the mass fraction of species  $k$ ;  $j_k$  is the flux of species  $k$ ;  $R_k$  is the rate expression for species  $k$  (kg/(m<sup>3</sup>·s));  $V_k$  is the multicomponent diffusion velocity of species  $k$  (m/s);  $D_k$  is the mixture averaged diffusion coefficient (m<sup>2</sup>/s);  $M_n$  is the mean molar mass of the gas mixture (kg/mol);  $z_k$  is the charge number of species  $k$ ;  $\mu_k$  is the mixture averaged mobility of species  $k$  (m<sup>2</sup>/(V s));  $E$  is the electric field strength (V/m). This paper takes into consideration  $M$  reactions ( $N$  two-body reactions and  $M-N$  three-body reactions) that change the mass fraction of species  $k$ ,

$$R_k = \frac{M_k}{N_A} \left( \sum_{j=1}^N k_j x_{j1} x_{j2} N_n^2 \Delta n_{kj} + \sum_{j=N+1}^M k_j x_{j1} x_{j2} x_{j3} N_n^3 \Delta n_{kj} \right) \quad (9)$$

$$x_k = \frac{M_n w_k}{M_k} \quad (10)$$

where  $x_{j1}$ ,  $x_{j2}$  and  $x_{j3}$  are the mole fractions of the species involved in reaction  $j$ ;  $N_A$  is the Avogadro constant;  $\Delta n_{kj}$  is the species  $k$  increment of reaction  $j$ ;  $M_k$  is the molar mass of species  $k$  (kg/mol). Eq. (9) shows the relationship between the mole fraction and mass fraction of species  $k$ .

The mixture averaged diffusion coefficient  $D_k$  is defined as Eq. (11) and the mixture averaged mobility  $\mu_k$  can be calculated by Eq. (12) according to the Einstein's relation,

$$D_k = \frac{1 - w_k}{\sum_{j \neq k}^Q x_j / D_{k,j}} \quad (11)$$

$$\mu_k = \frac{eD_k}{k_B T} \quad (12)$$

where  $e$  is the unit charge (C);  $k_B$  is the Boltzmann's constant (J/K);  $T$  is the gas temperature (K) and  $D_{k,j}$  is the binary diffusion coefficient between species  $k$  and  $j$ .

When electrons reach the conductor, the shell and the spacer surface, the boundary conditions for the electrons and electron energy flux can be defined as,

$$\vec{n} \cdot \vec{\Gamma}_e = \frac{1}{4} v_{e,th} n_e - \sum_p \gamma_p (\vec{\Gamma}_p \cdot \vec{n}) \quad (13)$$

$$\vec{n} \cdot \vec{\Gamma}_\varepsilon = \frac{5}{12} v_{e,th} n_e - \sum_p \varepsilon_p \gamma_p (\vec{\Gamma}_p \cdot \vec{n}) \quad (14)$$

$$v_{e,th} = \left( \frac{8k_B T_e}{\pi m_e} \right)^{1/2} \quad (15)$$

$$T_e = \frac{2n_\varepsilon}{3n_e} \quad (16)$$

The second term on the right-hand side of Eqs. (13) and (14) are the gain of electrons and electron energy due to secondary emission effects;  $\gamma_p$  is the secondary emission coefficient, which is set to 0.1 for the cathode and 0 for the anode;  $\varepsilon_p$  is the mean energy of the secondary electrons, which is set to 5 eV;  $v_{e,th}$  is the electron thermal velocity (m/s);  $T_e$  is the electron temperature (eV).

For ions, the boundary condition can be described as,

$$\vec{n} \cdot \vec{j}_k = \frac{1}{4} v_{k,th} \rho w_k + \alpha \rho w_k z_k \mu_k (\vec{E} \cdot \vec{n}) \quad (17)$$

$$v_{k,th} = \left( \frac{8k_B T}{\pi m_k} \right)^{1/2} \quad (18)$$

where  $v_{k,th}$  is the thermal velocity of species  $k$  (m/s);  $T$  can be considered to be the gas temperature in GIS (K);  $\alpha \bullet z_k / |z_k| = 0$  if the electric field is directed away from the boundary and  $\alpha \bullet z_k / |z_k| = 1$  if the electric field is directed toward the boundary.

The discharge processes of SF<sub>6</sub>/N<sub>2</sub> mixture are pretty complex and some of them are still unclear. In this simulation, only those primary reactions are taken into consideration. **Table 1** lists some typical physicochemical reactions considered in this paper after some reduction. The cross sections and energy losses of those collision reactions are extracted from papers [20–23].

### 2.3 Charge transport in epoxy spacer

When ions and electrons reach the spacer surface, charges are considered to be injected into the skin layer of epoxy owing to the surface reactions (N<sub>2</sub><sup>+</sup> → N<sub>2</sub>, SF<sub>6</sub><sup>+</sup> → SF<sub>6</sub>, SF<sub>6</sub><sup>−</sup> → SF<sub>6</sub>) [14]. The charge transport process in epoxy spacer volume is mainly controlled by the following equations (19)–(21) [24–26]. Note that the epoxy spacer in this numerical model is considered to be clean enough, the surface current due to surface transmission can be ignored since there is no special surface treatment to the spacer [27]. Therefore, the surface transmission process is not taken into consideration in this paper.

No.	Formula	Type	$\Delta\epsilon$ (eV)	$\Delta n_e$
1	$N_2 + e \rightarrow 2e + N_2^+$	Ionization	-16	1
2	$SF_6 + e \rightarrow 2e + SF_6^+$	Ionization	-15.8	1
3	$N_2 + e \rightarrow e + N_2$	Excitation	-8	0
4	$SF_6 + e \rightarrow e + SF_6$	Excitation	-10	0
5	$N_2 + e \rightarrow e + N_2$	Elastic	0	0
6	$SF_6 + e \rightarrow e + SF_6$	Elastic	0	0
7	$SF_6 + e \rightarrow SF_6^-$	Attachment	—	-1
8	$SF_6^+ + e \rightarrow SF_6$	Reaction	—	-1
9	$SF_6^+ + SF_6^- \rightarrow 2SF_6$	Reaction	—	—
10	$e + N_2^+ + N_2 \rightarrow 2N_2$	Reaction	—	-1
11	$2e + N_2^+ \rightarrow N_2 + e$	Reaction	—	-1

**Table 1.**  
*Table of some physicochemical reactions in the corona discharge.*

$$\frac{\partial n_{mb}}{\partial t} + \nabla \cdot \vec{J}_c^e = n_{tr}P_{de} - n_{mb}P_{tr} - R_1n_{mb}h_{tr} - \frac{1}{\tau}\Delta n \tag{19}$$

$$\frac{\partial n_{tr}}{\partial t} = n_{mb}P_{tr} - R_2n_{tr}h_{mb} \tag{20}$$

$$\vec{J}_c^e = \mu_{e,2}n_{mb} \cdot \nabla V - D_{e,2} \cdot \nabla n_{mb} \tag{21}$$

$$\frac{\partial h_{mb}}{\partial t} + \nabla \cdot \vec{J}_c^h = h_{tr}P_{de} - h_{mb}P_{tr} - R_2n_{tr}h_{mb} - \frac{1}{\tau}\Delta h \tag{22}$$

$$\frac{\partial h_{tr}}{\partial t} = h_{mb}P_{tr} - R_1n_{mb}h_{tr} \tag{23}$$

$$\vec{J}_c^h = -\mu_hh_{mb} \cdot \nabla V - D_h \cdot \nabla h_{mb} \tag{24}$$

where  $n_{mb}$  is the mobile electron density ( $1/m^3$ );  $n_{tr}$  is the trapped electron density ( $1/m^3$ );  $h_{mb}$  is the mobile hole density ( $1/m^3$ );  $h_{tr}$  is the trapped hole density ( $1/m^3$ );  $\vec{J}_c^e$  and  $\vec{J}_c^h$  are the flux of mobile electrons and holes ( $1/(m^2 \cdot s)$ );  $\mu_{e,2}$  and  $\mu_h$  are the mobility of electrons and holes in epoxy spacer ( $m^2/(V \cdot s)$ );  $D_{e,2}$  and  $D_h$  are the diffusion coefficient of electrons and holes ( $m^2/s$ );  $V$  is the potential (V);  $P_{tr}$  and  $P_{de}$  are the trapping and de-trapping coefficient of electrons and holes ( $1/s$ );  $\Delta n$  and  $\Delta h$  are the non-equilibrium carrier density in epoxy spacer ( $1/m^3$ );  $R_1$  and  $R_2$  are the recombination coefficients ( $m^3/s$ );  $\tau$  is the lifetime of non-equilibrium carriers (s).

In this paper, the volume conductivity, carrier mobility and diffusion coefficient of spacer are assumed as following:

$$\sigma = 40000 \cdot e^{-12860/T} \tag{25}$$

$$\mu_{e,2} = \mu_h = (1.5 \times 10^{-4}) \cdot e^{-6470/T} \tag{26}$$

$$D_{e,2} = D_h = \mu_{e,2} \cdot \frac{k_B T}{e} \tag{27}$$

where  $T$  is the temperature of spacer (K). Supposing the mobile electron density  $n_0$  and hole density  $h_0$  have the same value, the intrinsic carrier density can be described as,



$$n_0 = h_0 = \frac{\sigma}{2e\mu_{e,2}} \quad (28)$$

Inspired from the theories on the non-equilibrium carriers in the semiconductor physics, this paper considers the product of  $n_0$  and  $h_0$  as a constant in the epoxy spacer under thermal equilibrium condition. Supposing the electron and hole density  $n_{mb}$  and  $h_{mb}$  are in an unbalanced state,  $\Delta n$  and  $\Delta h$  can be obtained by solving the Eq. (29). Positive  $\Delta n$  and  $\Delta h$  represent the electron-hole recombination process, negative  $\Delta n$  and  $\Delta h$  represent the generation of electron-hole pairs.

$$n_0 h_0 = (n_{mb} - \Delta n)(h_{mb} - \Delta h) \quad (29)$$

$$\Delta n = \Delta h = \frac{1}{2} \left[ (n_{mb} + h_{mb}) - \sqrt{(n_{mb} - h_{mb})^2 + 4n_0 h_0} \right] \quad (30)$$

At the gas-solid interface, the boundary condition can be described as,

$$-\vec{n} \cdot \vec{\Gamma}_{n_{mb}} = \vec{n} \cdot \vec{j}_e \quad (31)$$

$$-\vec{n} \cdot \vec{\Gamma}_{h_{mb}} = \vec{n} \cdot \vec{j}_i \quad (32)$$

where  $\vec{j}_e$  and  $\vec{j}_i$  is the electron and ion flux through the gas-solid interface in the corona discharge model ( $1/\text{m}^2 \cdot \text{s}$ ).

At the metal-insulation interface, the boundary condition can be described as,

$$-\vec{n} \cdot \vec{j}_e = \alpha \cdot J_{sch-e} - (1 - \alpha) \cdot \vec{n} \cdot \vec{E} \cdot \mu_{e,2} \cdot n_{mb} \quad (33)$$

$$-\vec{n} \cdot \vec{j}_h = (1 - \alpha) \cdot J_{sch-h} - \alpha \cdot \vec{n} \cdot \vec{E} \cdot \mu_h \cdot h_{mb} \quad (34)$$

$$J_{sch-h} = J_{sch-h} = \frac{AT^2}{e} \cdot \exp \left( \frac{-\phi + \sqrt{E \cdot e^3 / 4\pi\epsilon_0\epsilon_r}}{k_B T} \right) \quad (35)$$

where  $J_{sch-e}$  and  $J_{sch-h}$  are the Schottky injection electron and hole flux ( $1/(\text{m}^2 \cdot \text{s})$ );  $A$  is the Richardson constant ( $\text{C}/\text{m}^2 \cdot \text{s} \cdot \text{K}^2$ ),  $\phi$  is the contact potential barrier between the spacer and metal (eV);  $\alpha = 0$  if the electric field is directed away from the boundary and  $\alpha = 1$  if the electric field is directed toward the boundary. **Table 2** lists some parameters of epoxy spacer used in the charge transport model.

Parameters	Value
Trapping and de-trapping coefficients, 1/s	
$P_{tr}$	$7.0 \times 10^{-3}$
$P_{de}$	$7.7 \times 10^{-5}$
Recombination coefficients, $\text{m}^3/\text{s}$	
$R_1$	$8.0 \times 10^{-19}$
$R_2$	$8.0 \times 10^{-19}$
Potential barrier, eV	
$\phi$	1.25

**Table 2.**

Table of some parameters in the charge transport model.

## 2.4 Poisson equation

The corona discharge model comprises  $p$  species (electrons, positive ions and negative ions) and the charged number of specie  $k$  is  $z_k$ . Thus, in the SF<sub>6</sub>/N<sub>2</sub> gas, Poisson equation can be described as,

$$-\nabla^2 V = e \left( \sum_1^p n_k z_k \right) / \epsilon_0 \quad (36)$$

where  $e$  is the elementary charge (C);  $n_k$  is the density of species  $k$  (1/m<sup>3</sup>);  $\epsilon_0$  is the vacuum dielectric constant (F/m).

In the epoxy spacer, Poisson equation is described as,

$$-\nabla^2 V = e(h_{mb} + h_{tr} - n_{mb} - n_{tr}) / (\epsilon_0 \epsilon_r) \quad (37)$$

where  $\epsilon_r$  is the relative dielectric constant of epoxy spacer, which is set to 4.

## 2.5 Heat transfer in GIS

In GIS, the heat transfer is controlled by the following equation [28],

$$\rho C_p \frac{\partial T}{\partial t} + \rho C_p \vec{u} \cdot \nabla T = \nabla \cdot (k \nabla T) + Q_\rho \quad (38)$$

$$\rho \frac{\partial \vec{u}}{\partial t} + \rho (\vec{u} \cdot \nabla) \vec{u} = \nabla \cdot \left[ -p \vec{I} + \mu \left( \nabla \vec{u} + (\nabla \vec{u})^T \right) - \frac{2}{3} \mu (\nabla \cdot \vec{u}) \vec{I} \right] + \vec{G} \quad (39)$$

$$\frac{\partial \rho}{\partial t} + \nabla \cdot (\rho \vec{u}) = 0 \quad (40)$$

where  $\rho$  is the density of SF<sub>6</sub>/N<sub>2</sub> gas, epoxy spacer or shell (kg/m<sup>3</sup>);  $C_p$  is the heat capacity (J/(kg·K));  $k$  is the thermal conductivity (W/(m·K));  $T$  is the thermodynamic temperature (K);  $\vec{u}$  is the natural convection velocity field of SF<sub>6</sub>/N<sub>2</sub> gas (m/s);  $\mu$  is the coefficient of kinetic viscosity, which is set to  $1.7 \times 10^{-5}$  Pa s;  $\vec{G}$  is the gravity vector (N/m<sup>3</sup>);  $Q_\rho$  is the heat source in the spacer (W/m<sup>3</sup>), which is defined as,

$$Q_\rho = eE^2 \mu (n_{mb} + h_{mb}) \quad (41)$$

The density of SF<sub>6</sub>/N<sub>2</sub> gas in GIS is defined as,

$$\rho = \frac{M_n p}{RT} \quad (42)$$

where  $M_n$  is the mean molar mass (kg/mol).

The heat radiation of conductor, spacer and shell is described as,

$$-\vec{n} \cdot (-k \nabla T) = \epsilon \sigma (T_{amb}^4 - T^4) \quad (43)$$

where  $\sigma$  is the Avogadro Boltzmann constant;  $T_{amb}$  is the environment temperature;  $\epsilon$  is the radiation coefficient, which is set to 0.8 for the spacer, 0.05 for the conductor and 0.15 for the shell.

In addition to the heat radiation at the shell-air interface, the natural convection of air can be described as,



Parameters	Spacer	Conductor/shell	SF <sub>6</sub> /N <sub>2</sub>
Thermal conductivity $k$ , W/(m K)	0.71	165	0.019
Heat capacity $C_p$ , J/(kg K)	700	900	817
Density $\rho$ , kg/m <sup>3</sup>	2200	2700	—

**Table 3.**  
*Table of some parameters in the heat transfer model.*

$$-\vec{n} \cdot (-k \nabla T) = h(T_0 - T) \tag{44}$$

where  $T_0$  is the environment temperature (K) and  $h$  is the heat transfer coefficient, which is set to 10 W/(m<sup>2</sup>·K). **Table 3** lists some parameters of GIS used in the heat transfer model.

Note that many simulation parameters such as  $\mu_{e,2}$ ,  $\mu_h$ ,  $D_{e,2}$ ,  $D_h$ ,  $P_{de}$ ,  $n_0$ ,  $v_{k,th}$ ,  $J_{sch-e}$ ,  $J_{sch-h}$ ,  $\rho$  and so on are all temperature-dependent. As a result, the temperature distribution has a great influence on the surface charge accumulation process. In this paper, the environment temperature is set to 293 K and the temperature of central conductor is respectively set to 330, 350 and 370 K.

3. Results and discussion

This paper built a temporal numerical model to simulate the surface charge accumulation process. But what should be cared about is the steady-state surface charge and electric field distributions. After many calculations, it can be drawn that the temporal change in surface charge density slows down with time under both negative and positive voltages. However, it takes a much longer time for the surface charge density to reach the steady state under negative voltage than that under positive voltage. For convenience, the simulation time is set to be 1 hour. After 1 hour, the increment of surface charge density has been slow enough. The difference between the surface charge distribution and the steady state is less than 10%. As a result, the surface charge density after 1 hour can be approximately considered as the steady-state distribution. It is necessary to note that it takes more than 20 hours for the measured surface charge distribution to reach the steady state [11, 12], which is much longer compared with the simulation. This phenomenon is mainly caused by the non-uniformity of material properties in the surface charge measurement.

3.1 Effects of surface charge

When GIS is under load condition, the central conductor has an obvious temperature rise due to joule heating. In this paper, the room temperature is set to 293 K. **Figure 2** shows the simulated temperature distribution and gas convection in DC-GIS when the conductor temperature is set to 350 K. The temperature goes down from the conductor to the shell and the shell temperature is about 17 K higher than the room temperature. Because of the gas convection, the spacer temperature is higher on the lower surface than that on the upper surface. There is a large temperature range along the epoxy spacers, thus it is important to study the temperature effects on the surface charge and electric field distribution.

**Figure 3** shows the simulated surface charge distribution on the basin-type spacer, which is similar to the measured results in paper [9, 11]. The conductor temperature is set to 350 K. The color variation from red to blue represents the

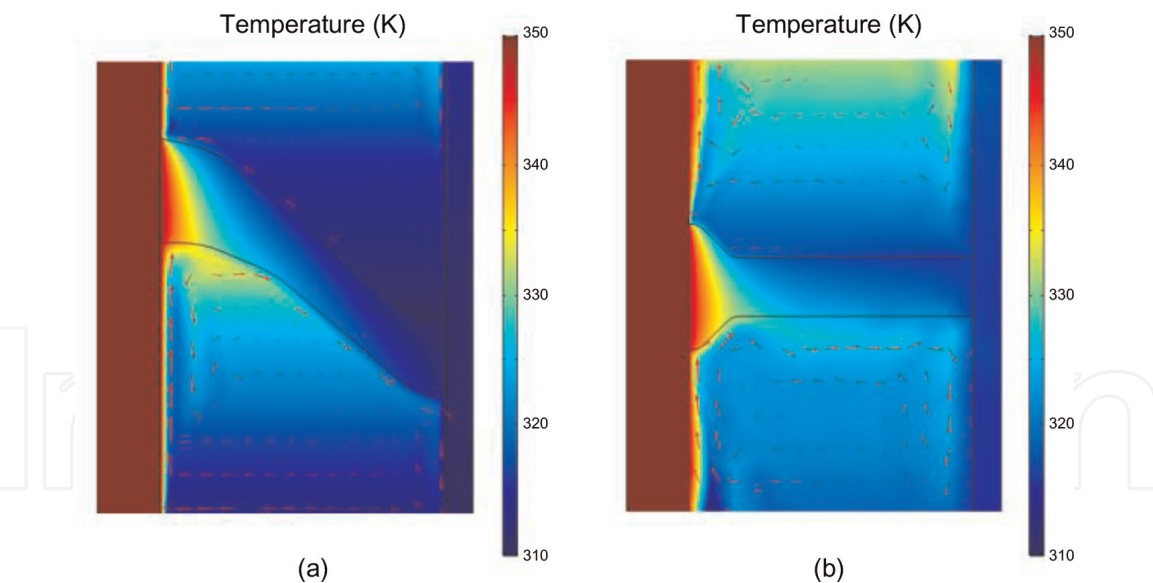


**Figure 2.**  
The simulated temperature distribution and gas convection in DC-GIS.

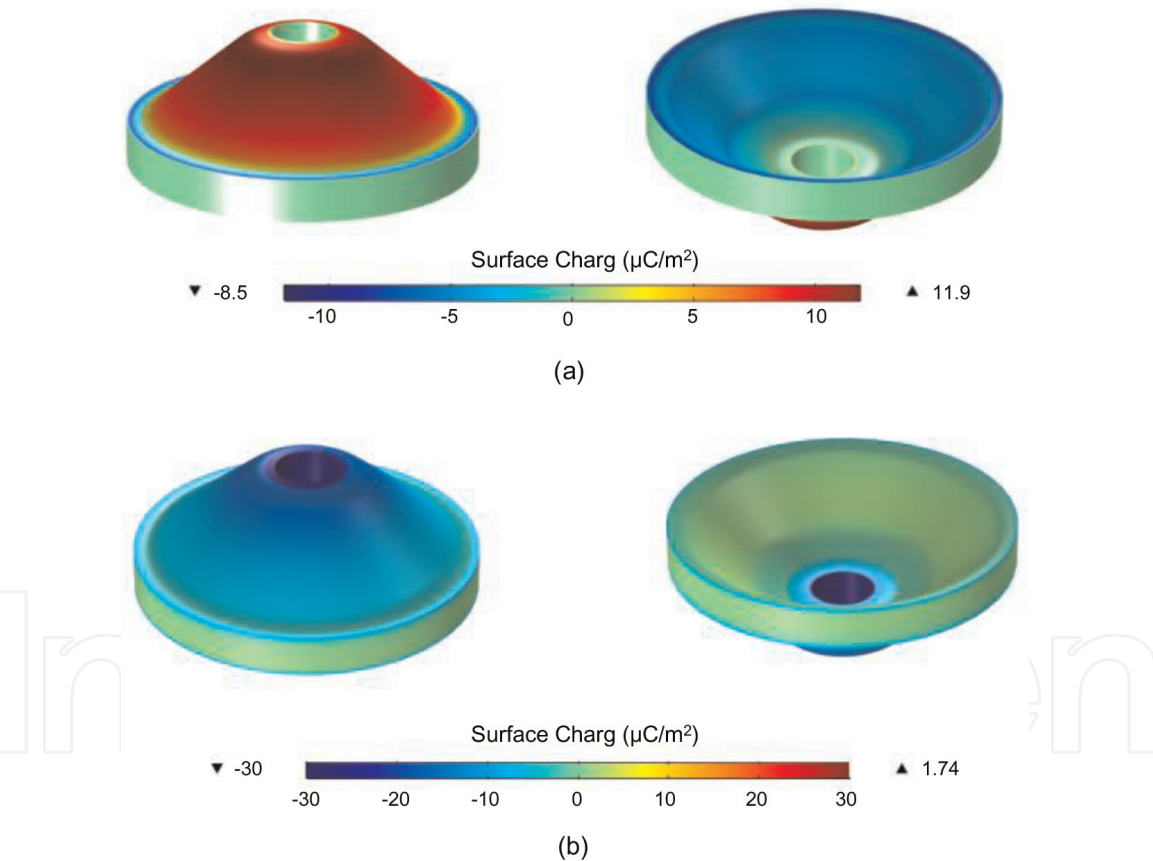


**Figure 3.**  
The simulated surface charge distribution on the basin-type spacer at 350 K: (a) negative voltage and (b) positive voltage.

conversion of surface charge polarity from positive to negative. In this paper, the convexity and concave of spacer are defined as the upper and lower surface. Generally speaking, the surface charge has the same polarity as the applied voltage on the lower surface but the opposite polarity on the upper surface. However, a density drop or even a polarity reversal of surface charge shows up near the central conductor.

**Figure 4** shows the mechanism of the surface charge accumulation process, which can be used to explain the surface charge distribution in **Figure 3**. Usually,

three processes are considered to influence the surface charge accumulation on GIS spacers. (1) Gas transmission: Ions and electrons produced by corona discharge in the insulating gas transport to the spacer surface by electric force; (2) Volume transmission: Carriers in the spacer volume transport to the spacer interface by electric force; (3) Surface transmission: Carriers transport along the spacer surface by electric force. In this paper, the spacer is considered to have a pretty clean surface, the surface transmission is thus not as influential as the gas and volume transmission.

As shown in **Figure 4** under negative voltage, electrons and negative ions in the  $\text{SF}_6/\text{N}_2$  mixture transport from the conductor to the shell and accumulate on the lower surface of spacer. Accordingly, the positive ions transport in the opposite direction and accumulate on the upper surface. In this case, the gas transmission takes the main part in the surface charge accumulation process. As a result, the surface charge has the same polarity as the applied voltage on the lower surface but the opposite polarity on the upper surface. When the conductor temperature is set to 350 K, there is a large temperature range along the spacer. According to the Eq. (25), the volume conductivity of spacer has been greatly increased near the central conductor. In this case, the volume transmission takes a more important role in the surface charge accumulation process. Electrons transport away from the conductor in the spacer volume and accumulate at the upper interface. Holes transport in the opposite direction and accumulate at the lower interface. This could explain why the density drop or the polarity reversal of surface charge shows up near the central conductor.

**Figure 5** shows the electric field distribution along the basin-type spacer under both negative and positive voltages. The temperature of conductor is set to 350 K. The coordinate  $r$  from 30 to 167 mm represents the spacer surface from the central conductor to the shell. In this paper, the electric field distribution without corona discharge is defined as the normal field. And the field distribution with corona discharge is defined as the distorted field. It can be seen that the normal field near the conductor is much weaker than that in the surrounding zone. This is induced by the greatly enhanced volume conductivity of spacer due to temperature rise on the

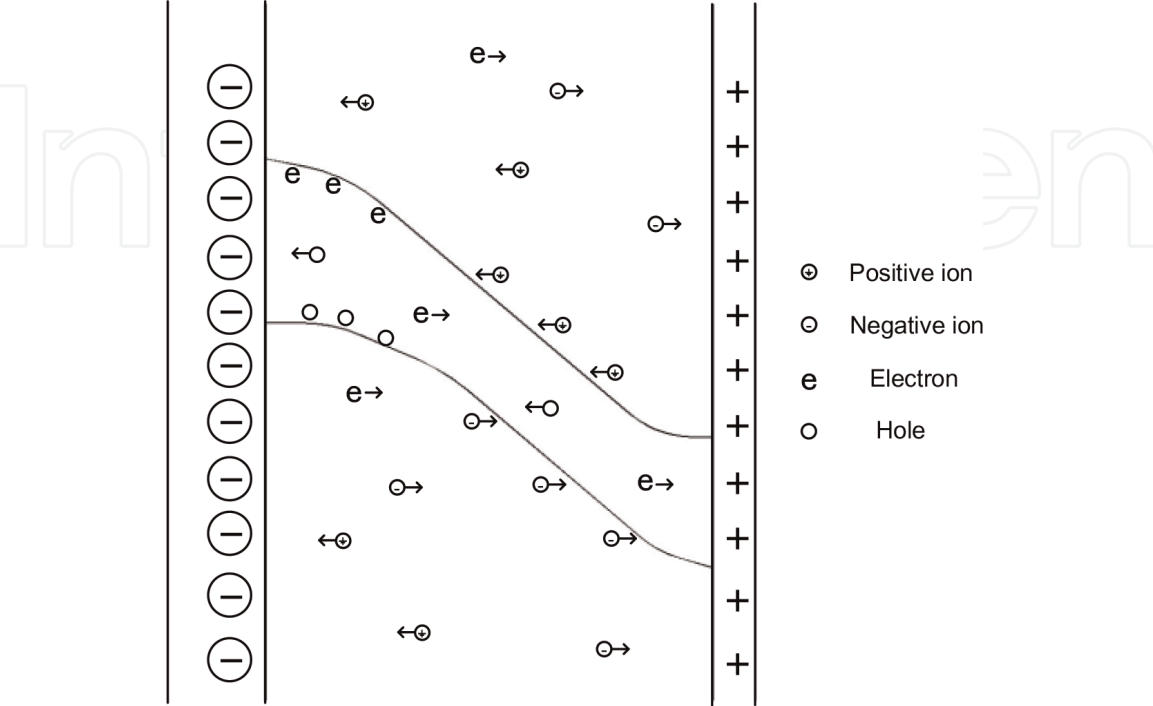


**Figure 4.**  
*Mechanism of the surface charge accumulation process.*

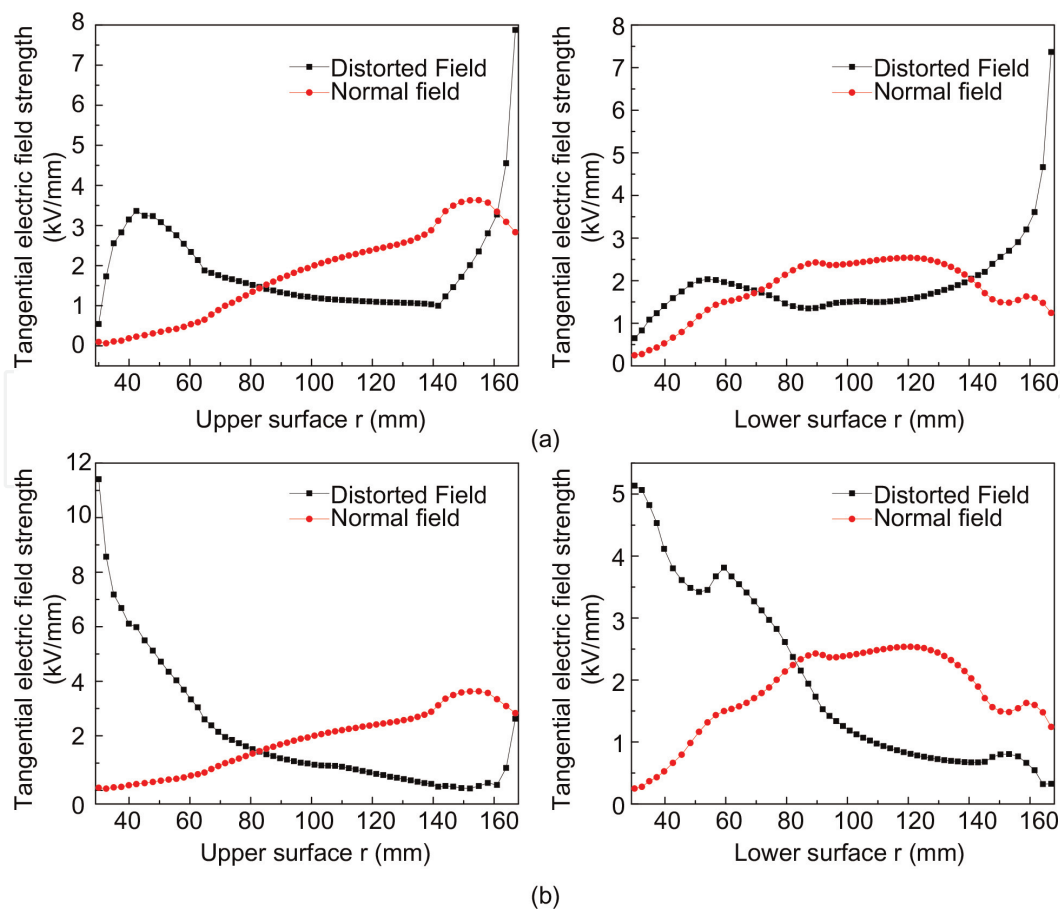


**Figure 5.**  
The electric field distribution along the basin-type spacer at 350 K: (a) negative voltage and (b) positive voltage.

conductor. When the corona discharge is taken into consideration, ions and electrons in the SF<sub>6</sub>/N<sub>2</sub> mixture will transport under electric force and accumulate on the spacer surface. Surface charge due to gas transmission can evidently distort the electric field. **Figure 5a** presents the distorted field distribution under negative voltage. The most serious distortion of electric field shows up in the zone close to the shell. From **Figure 3a** it can be learned that there is an annular zone with negative charge close to the shell. When negative voltage is applied on the conductor, the inner wall of the shell carries positive charges. Thus the existence of the negative charge zone greatly strengthens the electric field. **Figure 5b** presents the distorted field distribution under positive voltage. The most serious distortion of electric field shows up in the zone close to the conductor. Similarly, the negative charge zone surrounding the conductor should be responsible.

**Figure 6** shows the surface charge and the corresponding electric field distribution along the disc-type spacer under both negative and positive voltages. The temperature of conductor is set to 350 K. As shown in **Figure 6a** under negative voltage, the surface charge has the same polarity as the applied voltage near the shell but the opposite polarity near the conductor. But under positive voltage, negative surface charge exists almost on the whole surface. **Figure 6b** presents the normal and distorted field distribution under both negative and positive voltages. Without considering the corona discharge, the normal field near the conductor is weaker than that in the surrounding zone, which is similar as the field distribution along the basin-type spacer. The serious field distortion under negative voltage is induced by the negative charge zone close to the shell. And the serious field distortion under positive voltage is induced by the negative charge zone surrounding the conductor.



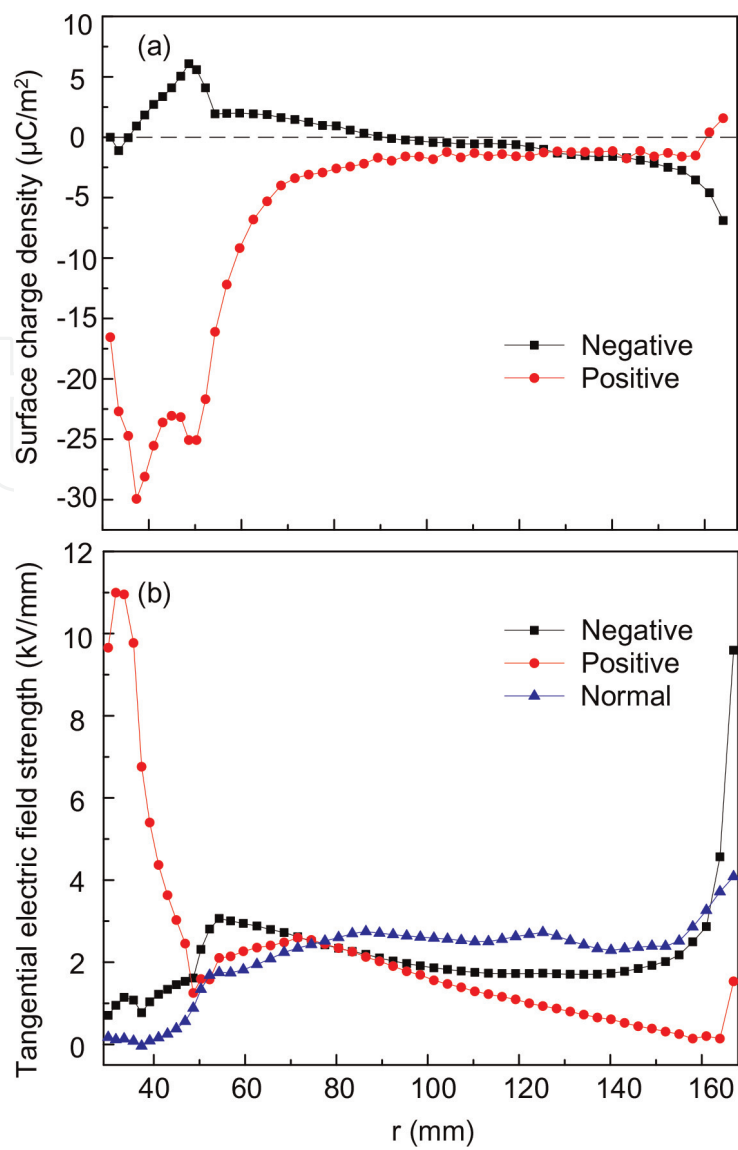


**Figure 6.** Surface charge and the corresponding electric field distribution along the disc-type spacer at 350 K: (a) surface charge and (b) electric field.

### 3.2 Effects of temperature

Under different load conditions, the conductor has different temperatures, leading to different temperature distributions in GIS. In this paper, many factors taken into consideration are temperature-dependent, such as carrier transport coefficient, carrier concentration, ion transport coefficient, Schottky injection current, gas density, thermal conductivity and so on. Therefore, temperature has a great influence on the surface charge accumulation process and the electric field distribution.

**Figure 7** shows the surface charge distribution along the basin-type spacer at different temperatures. Under negative voltage as shown in **Figure 7a**, less positive charges accumulate on the upper surface as the temperature increases. On the lower surface, the density of negative surface charge decreases with temperature and more positive charges are observed near the conductor. As the temperature increases, the conductivity of epoxy spacer grows up sharply. The volume transmission takes a more important role in the surface charge accumulation process. Similarly, under positive voltage as shown in **Figure 7b**, the volume transmission causes more positive charges to transport to the upper surface. Thus the negative surface charge due to gas transmission decreases with temperature. On the lower

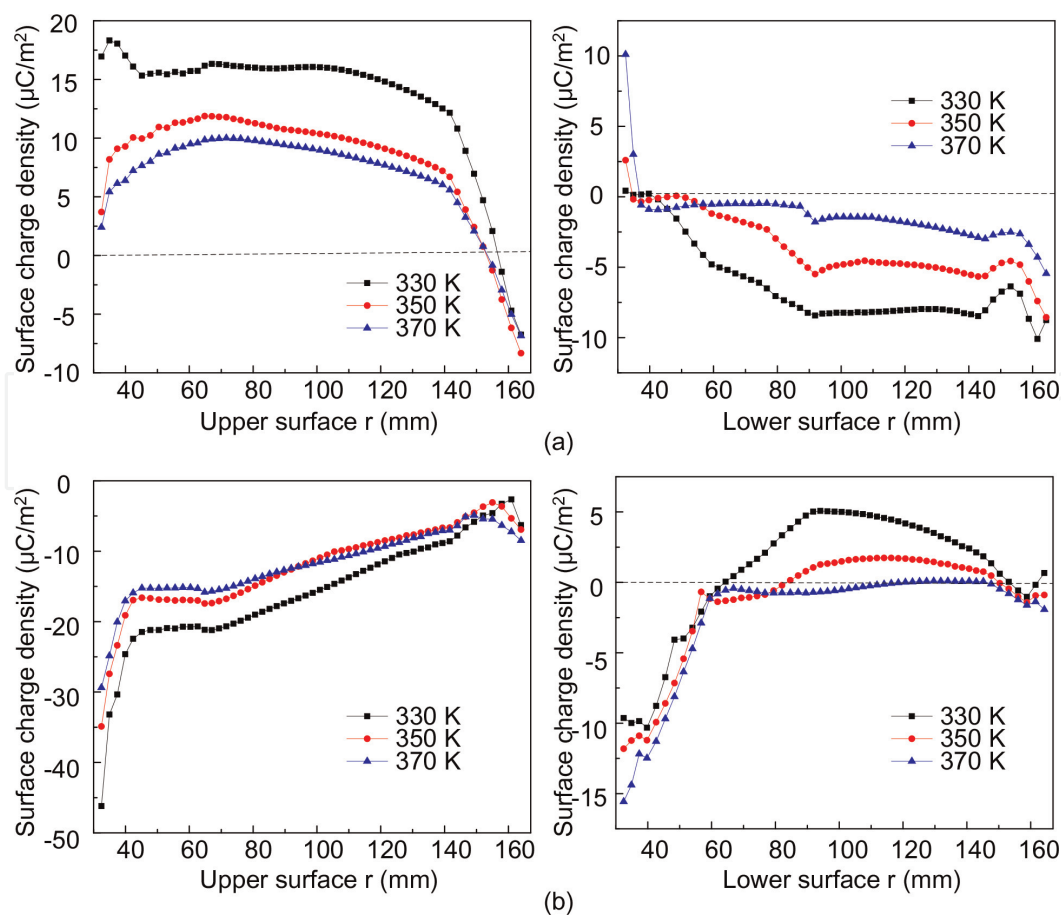


**Figure 7.**  
The surface charge distribution along the basin-type spacer at different temperatures: (a) negative voltage and (b) positive voltage.

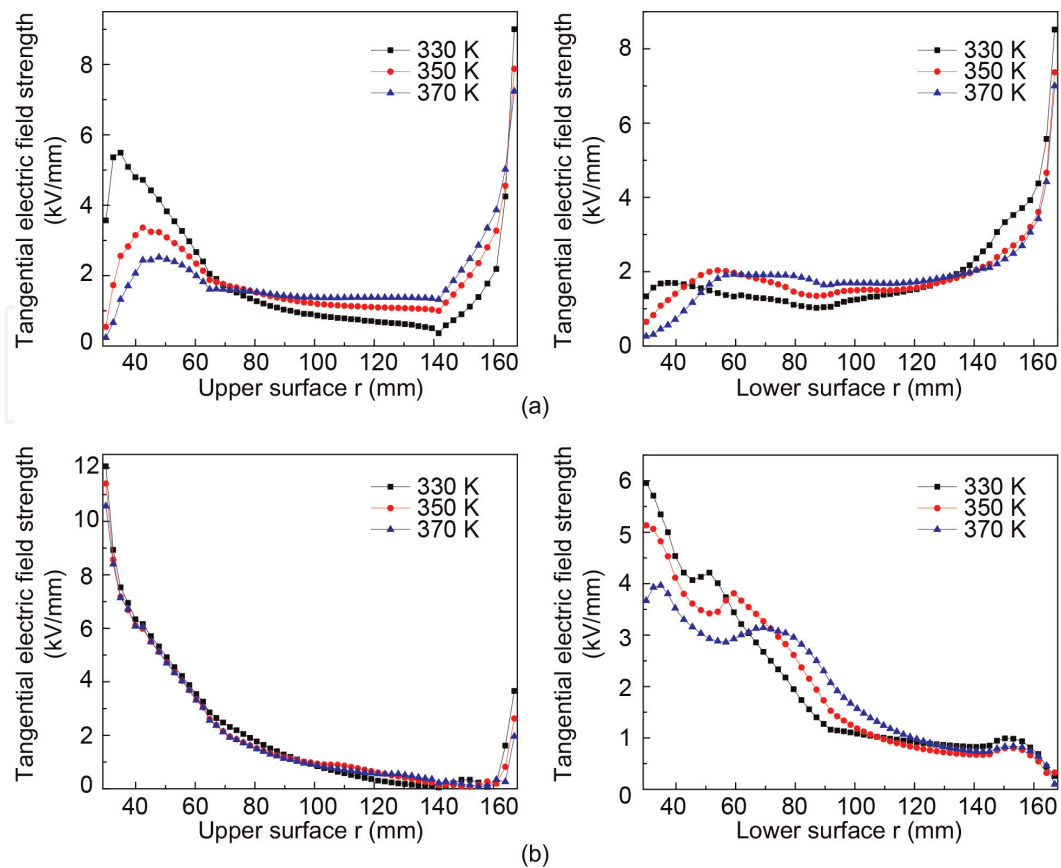


**Figure 8.**  
The distorted electric field distribution along the basin-type spacer at different temperatures: (a) negative voltage and (b) positive voltage.



surface, more negative charges and less positive charges are observed due to the enhanced volume transmissions as the temperature increases.

**Figure 8** shows the distorted electric field distribution along the basin-type spacer at different conductor temperatures. Under negative voltage as shown in **Figure 8a**, the field strength near the conductor is obviously decreased as the temperature increases. As the temperature goes up, the spacer has a huge temperature rise near the conductor, leading to the sharp increase in the volume conductivity. As a result, the grown volume conductivity greatly weakens the electric field near the conductor. Under positive voltage as shown in **Figure 8b**, the electric field near the conductor is also weakened with the increasing temperature, especially on the lower spacer surface. It seems that the heavy load on GIS is helpful to uniform the electric field distribution under positive voltage.

**Figure 9** shows the distorted electric field distribution along the disc-type spacer at different conductor temperatures. Similarly, the electric field is weakened near the conductor with the increasing temperature under both negative and positive voltages. This is induced by the temperature-dependent volume conductivity of epoxy spacer. When positive voltage is applied on the disc-type spacer, the huge temperature rise on the conductor is also considered to have the effect of field grading.

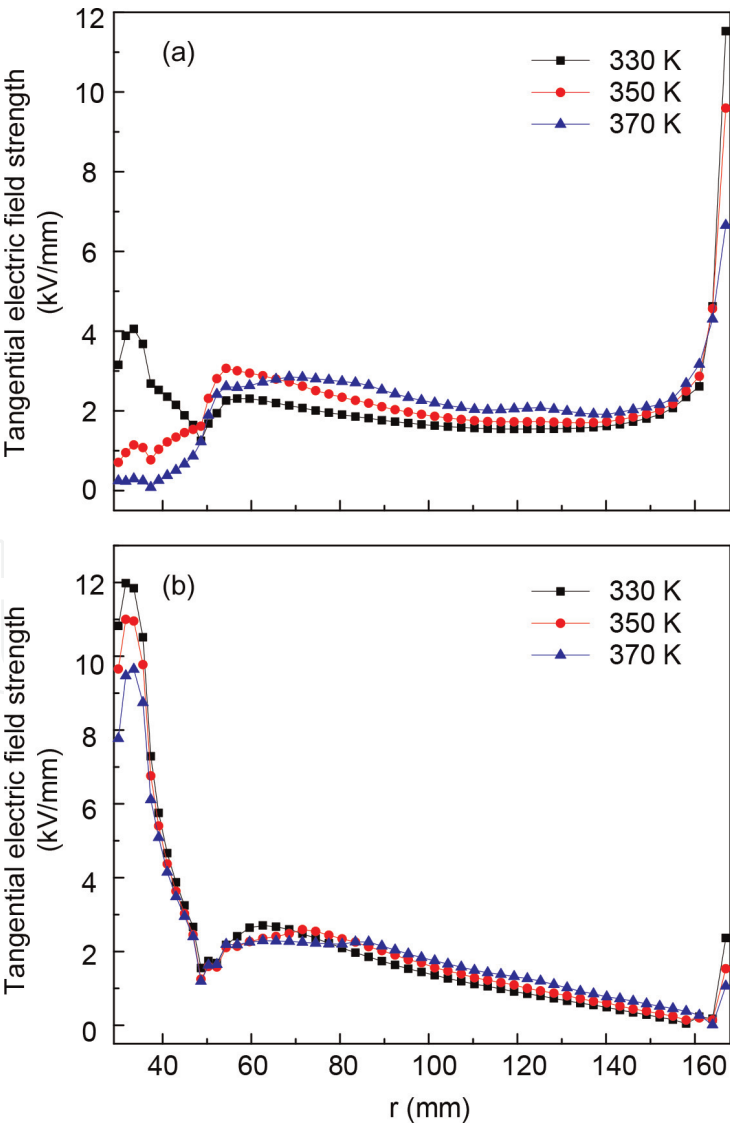


**Figure 9.**  
The distorted electric field distribution along the disc-type spacer at different temperatures. (a) negative voltage, (b) positive voltage.

3.3 Effects of shielding electrode

From the results in Section 3.1 it can be inferred that the most serious distortion of electric field occurs at the triple junction in GIS. On various occasions, the triple junction is always the cause of field distortion and partial discharge. In order to solve this problem, both the conductor and shell are designed with shielding structures as shown in **Figure 10**. Note that the grounded shielding electrode is designed

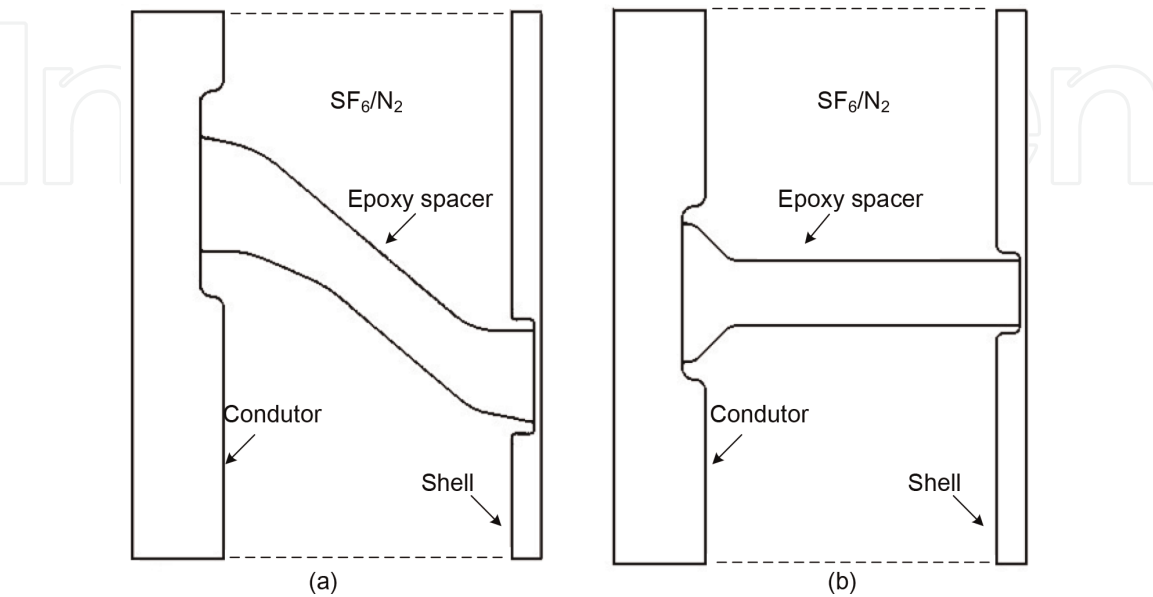


**Figure 10.**  
GIS with shielding structures on the conductor and shell. (a) basin-type spacer, (b) disc-type spacer.

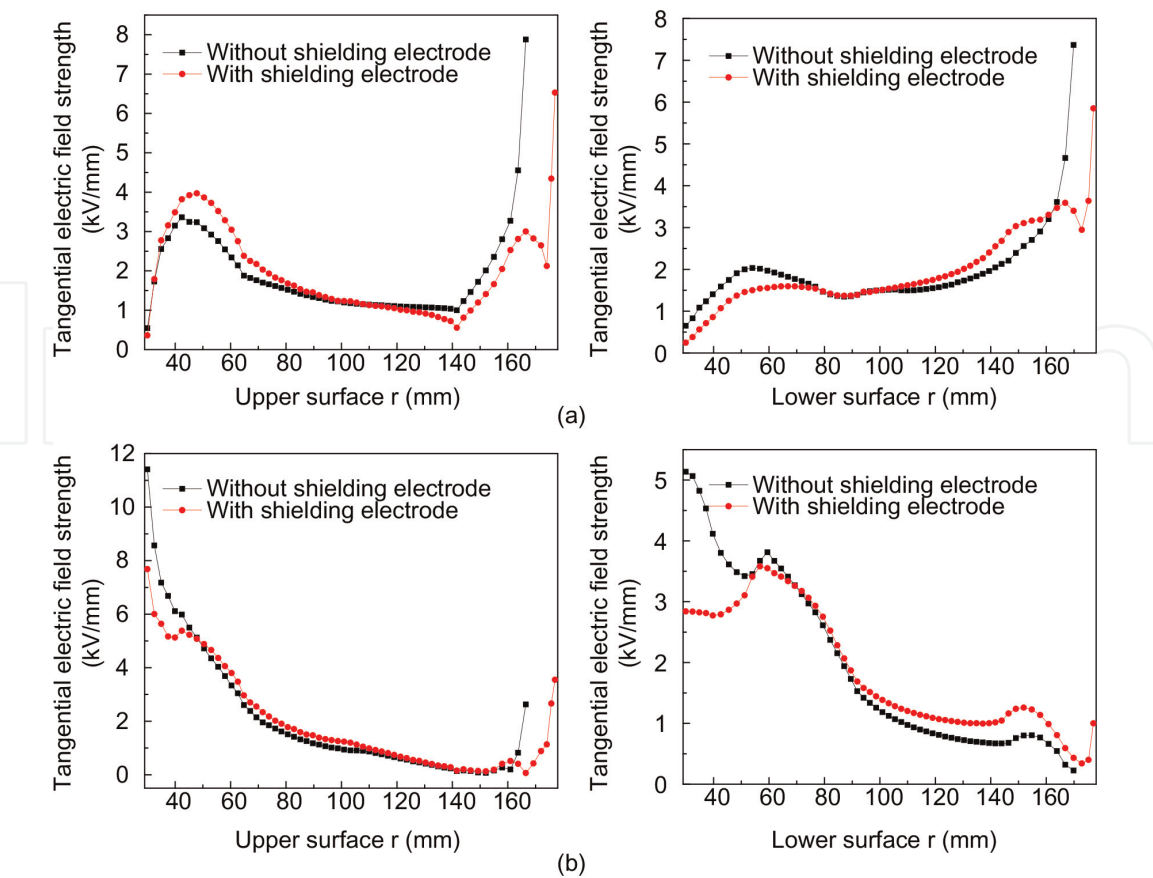


**Figure 11.**  
The electric field distribution along the basin-type spacer at 350 K with and without shielding electrodes: (a) negative voltage and (b) positive voltage.

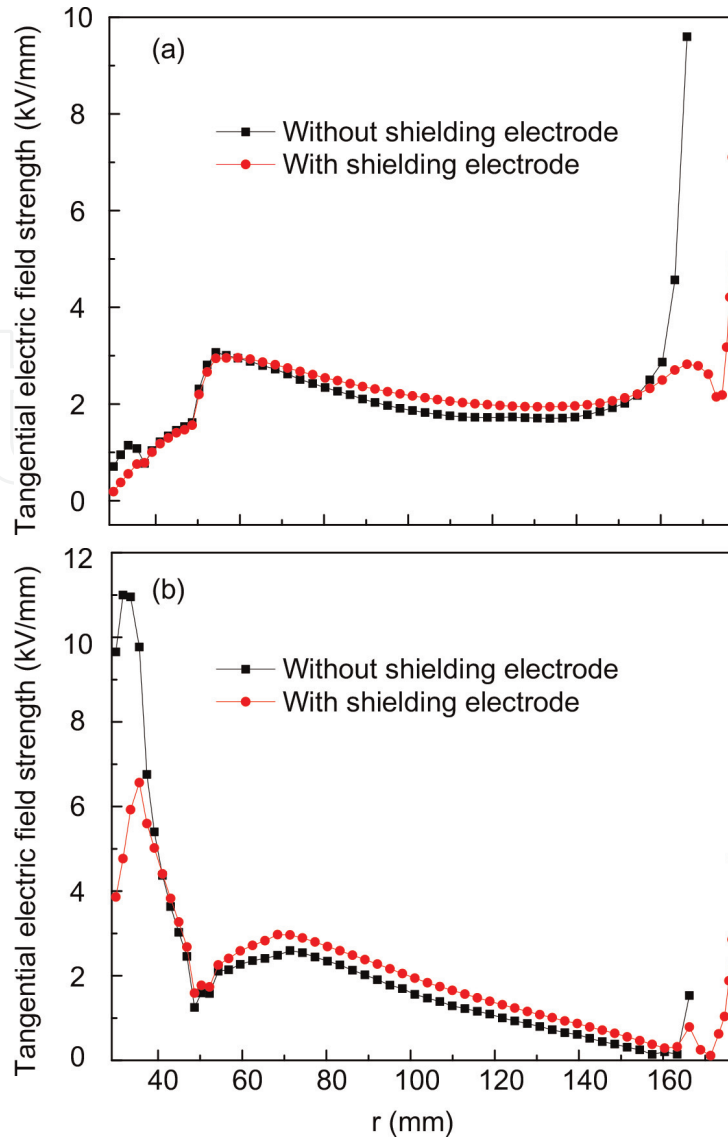


**Figure 12.**

The electric field distribution along the disc-type spacer at 350 K with and without shielding electrodes: (a) negative voltage and (b) positive voltage.

to be concave on the shell. As a result, the distance along the spacer surface from the conductor to the shell becomes a little longer.

**Figure 11** presents the comparison of electric field between the GIS with and without shielding electrodes. It is easy to find that the electric field distribution is greatly improved by the shielding electrodes. As mentioned above, the most serious distortion of electric field is induced by the negative surface charges at the triple junction. The existence of shielding electrodes prevents the charges from reaching the spacer surface at the triple junction. Besides, the uniformed electric field at the triple junction is considered to suppress the partial discharge, less surface charges are produced. **Figure 12** presents the electric field distribution along the disc-type spacer with and without shielding electrodes. Also, the electric field distribution along the disc-type spacer is uniformed by the shielding electrodes.

#### 4. Conclusions

This paper built a numerical model to simulate the surface charge accumulation process and the electric field distribution, the main conclusions can be drawn as follows:

1. Under load condition, there is a huge temperature rise on the GIS conductor due to joule heating. The wide variation of temperature along the epoxy spacers has a great influence on the surface charge accumulation process.
2. For the basin-type spacer, the surface charge has the same polarity as the applied voltage on the lower surface but the opposite polarity on the upper surface due to gas transmission. Because of the increasing spacer conductivity with temperature, the volume transmission takes a more important role in the surface charge accumulation process near the conductor. A density drop or even a polarity reversal of surface charge is observed near the conductor. For the disc-type spacer, the surface charge has the same polarity as the applied voltage near the shell but the opposite polarity near the conductor under negative voltage. But under positive voltage, negative charge exists almost on the whole surface.
3. The most serious distortion of the electric field distribution along the epoxy spacers occurs at the triple junction. As the conductor temperature increases, the field strength near the conductor is weakened owing to the temperature-dependent volume conductivity.
4. The application of shielding electrodes has the function of field grading at the triple junction, which can be referred in the DC-GIS/GIL design.


IntechOpen

### Author details

Boxue Du, Jin Li\* and Hucheng Liang  
Key Laboratory of Smart Grid of Education Ministry, School of Electrical and Information Engineering, Tianjin University, Tianjin, China

\*Address all correspondence to: [lijin@tju.edu.cn](mailto:lijin@tju.edu.cn)

### IntechOpen

© 2019 The Author(s). Licensee IntechOpen. This chapter is distributed under the terms of the Creative Commons Attribution License (<http://creativecommons.org/licenses/by/3.0>), which permits unrestricted use, distribution, and reproduction in any medium, provided the original work is properly cited. 

## References

- [1] Delucchi MA, Jacobson MZ. Providing all global energy with wind, water, and solar power, Part II: Reliability, system and transmission costs, and policies. *Energy Policy*. 2011; **39**(3):1170-1190. DOI: 10.1016/j.enpol.2010.11.045
- [2] Liu Y, Li C, Mu Q, et al. Side-by-side connection of LCC-HVDC links to form a DC grid. In: *European Conference on Power Electronics and Applications*. IEEE. 2015. pp. 1-10. DOI: 10.1109/EPE.2015.7311787
- [3] Du BX, Li A. Effects of DC and pulse voltage combination on surface charge dynamic behaviors of epoxy resin. *IEEE Transactions on Dielectrics & Electrical Insulation*. 2017; **24**(4):2025-2033. DOI: 10.1109/TDEI.2017.006164
- [4] Du BX, Li A, Li J. Effects of AC and pulse voltage combination on surface charge accumulation and decay of epoxy resin. *IEEE Transactions on Dielectrics & Electrical Insulation*. 2016; **23**(4): 2368-2376. DOI: 10.1109/TDEI.2016.7556515
- [5] Lin C, Li C, He J, et al. Surface charge inversion algorithm based on bilateral surface potential measurements of cone-type spacer. *IEEE Transactions on Dielectrics & Electrical Insulation*. 2017; **24**(3):1905-1912. DOI: 10.1109/TDEI.2017.006496
- [6] Du BX, Liang HC, Li J, et al. Temperature-dependent surface potential decay and flashover characteristics of epoxy/SiC composites. *IEEE Transactions on Dielectrics & Electrical Insulation*. 2018; **25**(2): 631-638. DOI: 10.1109/TDEI.2017.006872
- [7] Liang HC, Du BX, Li J, et al. Effects of nonlinear conductivity on charge trapping and de-trapping behaviors in epoxy/SiC composites under dc stress. *IET Science Measurement & Technology*. 2018; **12**(1):83-89. DOI: 10.1049/iet-smt.2016.0528
- [8] Liang HC, Du BX, Li J, et al. Numerical simulation on the surface charge accumulation process of epoxy insulator under needle-plane corona discharge in air. *IET Science Measurement & Technology*. 2018; **12**(1):9-16. DOI: 10.1049/iet-smt.2017.0164
- [9] Vu-Cong T, Zavattoni L, Vinson P, et al. Surface charge measurements on epoxy spacer in HVDC GIS/GIL in SF<sub>6</sub>. *IEEE Electrical Insulation and Dielectric Phenomena*. 2016. DOI: 10.1109/CEIDP.2016.7785506
- [10] Nakanishi K, Yoshioka A, Arahata Y, et al. Surface charging on epoxy spacer at DC stress in compressed SF<sub>6</sub> Gas. *IEEE Power Engineering Review*. 1983; **PER-3**(12):46-46. DOI: 10.1109/MPER.1983.5520154
- [11] Zhang B, Qi Z, Zhang G. Charge accumulation patterns on spacer surface in HVDC gas-insulated system: Dominant uniform charging and random charge speckles. *IEEE Transactions on Dielectrics & Electrical Insulation*. 2017; **24**(2):1229-1238. DOI: 10.1109/TDEI.2017.006067
- [12] Zhang B, Qi Z, Zhang G. Thermal gradient effects on surface charge of HVDC spacer in gas insulated system. *IEEE Electrical Insulation and Dielectric Phenomena*. 2016. DOI: 10.1109/CEIDP.2016.7785563
- [13] Zhou HY, Ma GM, Li CR, et al. Impact of temperature on surface charges accumulation on insulators in SF<sub>6</sub>-filled DC-GIL. *IEEE Transactions on Dielectrics & Electrical Insulation*. 2017; **24**(1):601-610. DOI: 10.1109/TDEI.2016.005838
- [14] Sato S, Zaengl WS, Knecht A. A numerical analysis of accumulated



surface charge on DC epoxy resin spaces. *IEEE Transactions on Electrical Insulation*. 2007;**22**(3):333-340. DOI: 10.1109/TEI.1987.298999

[15] Lutz B, Kindersberger J. Surface charge accumulation on cylindrical polymeric model insulators in air: Simulation and measurement. *IEEE Transactions on Dielectrics & Electrical Insulation*. 2012;**18**(6):2040-2048. DOI: 10.1109/TDEI.2011.6118642

[16] Winter A, Kindersberger J. Stationary resistive field distribution along epoxy resin insulators in air under DC voltage. *IEEE Transactions on Dielectrics & Electrical Insulation*. 2012; **19**(5):1732-1739. DOI: 10.1109/TDEI.2012.6311522

[17] Winter A, Kindersberger J. Transient field distribution in gas-solid insulation systems under DC voltages. *IEEE Transactions on Dielectrics & Electrical Insulation*. 2014;**21**(1): 116-128. DOI: 10.1109/TDEI.2013.004110

[18] He W, Liu XH, Yang F, et al. Numerical simulation of direct current glow discharge in air with experimental validation. *Japanese Journal of Applied Physics*. 2012;**51**(51):6001. DOI: 10.1143/JJAP.51.026001

[19] Hagelaar GJM. Solving the Boltzmann equation to obtain electron transport coefficients and rate coefficients for fluid models. *Plasma Sources Science & Technology*. 2005; **14**(4):722-733. DOI: 10.1088/0963-0252/14/4/011

[20] Christophorou LG, Brunt RJV. SF<sub>6</sub>//N<sub>2</sub> mixtures: Basic and HV insulation properties. *IEEE Transactions on Dielectrics & Electrical Insulation*. 2002;**2**(5):952-1003. DOI: 10.1109/94.469988

[21] Itikawa Y. Cross sections for electron collisions with nitrogen molecules. *Journal of Physical &*

*Chemical Reference Data*. 2006;**35**(1): 31-53. DOI: 10.1063/1.1937426

[22] Gulley RJ, Cho H, Buckman SJ. The total elastic cross section for electron scattering from SF<sub>6</sub>. *Journal of Physics B: Atomic, Molecular and Optical Physics*. 2000;**33**(8):L309-L315. DOI: 10.1088/0953-4075/33/8/105

[23] Phelps AV, Van Brunt RJ. Electron-transport, ionization, attachment, and dissociation coefficients in SF<sub>6</sub> and its mixtures. *Journal of Applied Physics*. 1988;**64**(9):4269-4277. DOI: 10.1063/1.341300

[24] Zhou TC, Chen G, Liao RJ, et al. Charge trapping and detrapping in polymeric materials. *Journal of Applied Physics*. 2009;**106**(12):644-637. DOI: 10.1063/1.3273491

[25] Chen G, Zhao J, Zhuang Y. Numerical modeling of surface potential decay of corona charged polymeric material. *IEEE International Conference on Solid Dielectrics*. 2010:1-4. DOI: 10.1109/ICSD.2010.5567997

[26] Min DM, Li ST, Li GC. The effect of charge recombination on surface potential decay crossover characteristics of LDPE. In: *International Symposium on Electrical Insulating Materials*. 2014. pp. 104-107. DOI: 10.1109/ISEIM.2014.6870731

[27] Straumann U, Schuller M, Franck CM. Theoretical investigation of HVDC disc spacer charging in SF<sub>6</sub> gas insulated systems. *IEEE Transactions on Dielectrics & Electrical Insulation*. 2013; **19**(6):2196-2205. DOI: 10.1109/TDEI.2012.6396980

[28] Wang Q, Wang H, Peng Z, et al. 3-D coupled electromagnetic-fluid-thermal analysis of epoxy impregnated paper converter transformer bushings. *IEEE Transactions on Dielectrics & Electrical Insulation*. 2017;**24**(1): 630-638. DOI: 10.1109/TDEI.2016.005641